7. D. H. Stedman et al., "On-road carbon monoxide and hydrocarbon remote sensing in the Chicago area: Final report" (ILENR/RE-AQ-91/14, Illinois Department of Energy and Natural Resources, Office of Research and Planning, Springfield, IL, 1991).

8. D. H. Stedman, G. Bishop, J. E. Peterson, P. L. Guenther, "On-road CO remote sensing in the Los Angeles Basin: Final report" (California Air Resources Board, Sacramento, CA, 1991).

9. R. D. Stephens and S. H. Cadle, J. Air Waste Manage. Assoc. 41, 39 (1991).

10. L. L. Ashbaugh et al., paper presented at Air and Waste Management Association/Environmental Protection Agency Conference, "PM$_{10}$ standards and nontraditional particulate source controls," Phoenix, AZ, 12 to 15 January 1992.

11. D. Elliott, C. Kaskavaltizis, T. Topaloglu, Society of Automotive Engineers paper 922314, presented at International Fuels and Lubricants Meeting and Exposition, San Francisco, 19 to 22 October 1992.

12. D. L. Smith and P. M. McClintock, Society of Automotive Engineers paper 922313, presented at International Fuels and Lubricants Meeting and Exposition, San Francisco, 19 to 22 October 1992.

13. K. A. Whitney and E. L. Glover, Society of Automotive Engineers paper 922315, presented at International Fuels and Lubricants Meeting and Exposition, San Francisco, 19 to 22 October 1992.

14. E. M. Fujita, B. E. Croes, F. W. Lurmann, paper presented at Coordinating Research Council–Air Pollution Research Advisory Committee Vehicle Emission Modeling Workshop, Newport Beach, CA, 30 and 31 October 1990.

15. R. A. Harley, A. G. Russell, G. J. McRae, G. R. Cass, J. H. Seinfeld, Environ. Sci. Technol. 27, 378 (1993).

16. A. W. Gertler, W. R. Pierson, B. Zlelinska, J. C. Sagebiel, R. V. Zweldinger, paper presented at Coordinating Research Council–Air Pollution Research Advisory Committee Third Annual On-Road Vehicle Emissions Workshop, San Diego, 1 to 3 December 1992.

17. W. R. Pierson and A. W. Gertler, "SORP-EE tunnel study for measurement of vehicle emissions," Revised Program Plan, Desert Research Institute document no. 8630.1F1 (prepared for E. B. Cowling, College of Forest Resources, North Carolina State University, Raleigh, NC; T. C. Belian, Coordinating Research Council, Atlanta, GA; K. T. Knapp, Chief, Mobile Source Emissions Research Branch) (U.S. Environmental Protection Agency, Research Triangle Park, NC, 1992).

18. W. R. Pierson, N. F. Robinson, A. W. Gertler, paper presented at Southern California Air Quality Study Data Analysis Conference, University of California at Los Angeles, 21 to 23 July 1992.

19. A. M. Dunker et al., Air and Waste Management Association paper 92-119.03, presented at AWMA Annual Meeting, Kansas City, MO, 21 to 26 June 1992.

20. The RVP defines a fuel's low-end volatility and is the vapor pressure of an air-to-fuel ratio of 4:1 at 100°F.

21. "Effects of fuel sulfur on mass exhaust emissions, air toxics, and reactivity," Technical Bulletin No. 8 (Auto/Oil Air Quality Improvement Research Program, Coordinating Research Council, Atlanta, GA, 1992).

22. "Effects of heavy hydrocarbons on exhaust emissions," Preliminary Report (Auto/Oil Air Quality Improvement Research Program, Coordinating Research Council, Atlanta, GA, 1993).

23. 1992 Motor Vehicle Manufacturers' Association Summer Gasoline Survey (American Automobile Manufacturers Association, Detroit, 1992).

24. "A study of fuel effects on emissions from high emitting vehicles," Technical Bulletin no. 11 (Auto/Oil Air Quality Improvement Research Program, Coordinating Research Council, Atlanta, GA, 1992).

25. A. A. Quader, T. M. Sloane, R. M. Sinkevitch, K. L. Olson, Society of Automotive Engineers paper 912430, presented at Society of Automotive Engineers International Fuels and Lubricants Meeting, Toronto, 7 to 10 October 1991.

26. T. A. Renner, J. C. Knepper, G. A. Huff, Jr., J. T. Hargreaves, Society of Automotive Engineers paper 930371, presented at 1993 Society of Automotive Engineers International Congress, Detroit, 1 to 5 March 1993.

27. A. M. Dunker, C. H. Schleyer, R. E. Morris, A. K. Pollack, Air and Waste Management Association paper 92-119.06, presented at AWMA Annual Meeting, Kansas City, MO, 21 to 26 June 1992.

28. L. H. Browning and C. B. Moyer, Screening Study of Mobile-Source Strategies for the Northeast, (Acurex Environmental Corporation, Mountain View, CA, 1992).

29. L. L. Ashbaugh, B. E. Croes, E. M. Fujita, D. R. Lawson, paper presented at the 13th North American Motor Vehicle Emissions Control Conference, Tampa, FL, 13 December 1990.

Geophysical Investigations of the Tectonic Boundary Between East and West Antarctica

U. S. ten Brink, S. Bannister, B. C. Beaudoin, T. A. Stern

The Transantarctic Mountains (TAM), which separate the West Antarctic rift system from the stable shield of East Antarctica, are the largest mountains developed adjacent to a rift. The cause of uplift of mountains bordering rifts is poorly understood. One notion based on observations of troughs next to many uplifted blocks is that isostatic rebound produces a coeval uplift and subsidence. The results of an over-snow seismic experiment in Antarctica do not show evidence for a trough next to the TAM but indicate the extension of rifted mantle lithosphere under the TAM. Furthermore, stretching preceded the initiation of uplift, which suggests thermal buoyancy as the cause for uplift.

Our knowledge of the tectonic history of Antarctica is largely based on information from the surrounding continents, ocean basins, and the continental margins of Antarctica. With the exception of the open waters of the Ross and the Weddell seas and a few rock outcrops, Antarctic geology is buried under a thick ice cover and can only be studied by geophysical methods that remotely sense the Earth's crust under the ice. These geophysical methods include the measurement of subglacial topography by radar, the measurement of anomalies in the Earth's gravity and magnetic fields, and magnetotelluric and seismic methods. Ground and aerial radar and magnetic surveys and ground surveys of gravity have been carried out in Antarctica during the past 20 years (1, 2). An integrated survey including radar, magnetic, and gravity measurements from a small aircraft has been attempted (3). Although seismic methods are the primary geophysical tool elsewhere in the world, only a few over-snow seismic surveys have been conducted in Antarctica (4) because surveys there are limited to crevasse-free areas and can be done only with substantial logistical support.

Stretching and breakup of the continental lithosphere are the fundamental geolog-

ical process that creates rift basins and, eventually, oceans. The process should be manifested in the crustal structure of the transition zone between rifts and oceans and the stable continent. In Antarctica, the transition from the West Antarctic rift (which includes the Ross Embayment) to the East Antarctica shield involved the formation of a rift-flank mountain range, a phenomenon that is not well understood. Both the area of the rift and the size of the flanking mountains, the 3500-km-long and the 4500-m-high TAM, are among the largest in the world (Figs. 1 and 2). In this article, we present results from Seismic Experiment Ross Ice Shelf (SERIS), a large-scale, modern multichannel seismic reflection and refraction experiment over the snow in Antarctica (Fig. 2). This experiment took place in the austral summer of 1990 to 1991 and examined the geometry of the boundary between the West Antarctic rift system and East Antarctica as well as the causes for the uplift of the TAM.

Tectonic History

Before the breakup of the Gondwana supercontinent in the early Jurassic [~175 million years ago (Ma)], Antarctica lay at the center of this land mass (Fig. 1) (5) and so is the key to an understanding of Gondwana geology and plate reconstruction. The continent now consists of two major parts: East Antarctica, a large stable block that has existed relatively intact for hundreds of millions of years, and West Antarctica, an

U. S. ten Brink is with the U.S. Geological Survey, Woods Hole, MA 02543. S. Bannister is with the Institute of Geological and Nuclear Sciences, Wellington, New Zealand. B. C. Beaudoin is with the Department of Geophysics, Stanford University, Stanford, CA 94305. T. A. Stern is with the Research School of Earth Sciences, Victoria University, Wellington, New Zealand.

assemblage of smaller blocks including Marie Byrd Land, Thurston Island, Ellsworth-Whitmore Mountains, and the Antarctic Peninsula that have been moving relative to one another and to East Antarctica during the last 230 million years (Fig. 1) (6). It has been suggested that the early stages of the breakup of Gondwana involved rifting or strike-slip between East and West Antarctica. The process of rifting explains the linear distribution of the voluminous Ferrar dolerites along the TAM (7), and strike-slip faulting can account for the 90° counterclockwise rotation of the Ellsworth-Whitmore block away from East Antarctica (6). However, no basins associated with this early stage have been identified.

West Antarctica was attached to New Zealand until 72 Ma (Fig. 1) (8). Before 105 ± 5 Ma, subduction of oceanic lithosphere took place along the Gondwana margin of New Zealand and along the Antarctic Peninsula (9). Rifting and stretching began almost immediately after the end of subduction (5, 9), as evidenced by rapid subsidence off the shore of New Zealand at ~100 Ma (10). The similar crustal structures of the Ross Embayment and the Campbell Plateau of New Zealand (11) suggest that much stretching in the Ross Embayment occurred before final separation. Seismic stratigraphic evidence from the Ross Sea, the most accessible part of the West Antarctic rift system, indicates that rifting occurred in at least two

phases. The first was a widespread event during the late Mesozoic, and the second was a late Cenozoic event concentrated in the Terror rift close to the TAM (12). The second event was also accompanied by basaltic volcanism along part of the TAM and in Marie Byrd Land (13).

The TAM, like other rift-flank mountains such as those along Southeast Australia, the west side of India, the rim of southern Africa, and the Red Sea coasts (14), lack compressional deformation and have an asymmetric topographic profile—an escarpment facing the rift and a gentle slope away from it. Fission track studies indicate that denudation (presumably resulting from uplift) of the TAM north of latitude 85°S started at 55 Ma (15), but the rate of uplift is controversial (13, 16). Unlike the formation of cordilleran (the Andes) and collision-type mountains (the Himalayas) that result from horizontal compression, formation of mountains alongside rifts is poorly understood. Several models have been proposed. Specifically, the proximity of the Terror rift to the mountains (Fig. 2) led Stern and ten Brink (14, 17) to model the lithospheres of East Antarctica and West Antarctica as two cantilevered elastic beams that were free to move with respect to each other at their adjoining boundary (Fig. 3) (17). The East Antarctic side was modeled as being curled up (or flexed) at its edge to form an asymmetric topographic profile with the flexed edge representing the TAM. The calculated profile of the flexed beam was compared to five sub-ice topographic profiles across the mountains, and the fit was remarkably good (17). Such an approach is possible because the ice cover during part of the Tertiary helped preserve much of the original land topography (14). The fit of the down-flexed beam to the bathymetry of the Ross Embayment was less convincing (17).

One conclusion from the elastic-beam model was that a broad and shallow depression should have formed behind and parallel to the mountains (Fig. 3) (14). The distance from the mountain front to the axis of the hinterland basin constrains the rigidity of the lithosphere, which is related

Fig. 1. Reconstruction of Gondwana at 118 Ma (5). Circles enclose West Antarctica. Barbed line, subduction of oceanic lithosphere under the Gondwana margin (9); inverted "V"s, TAM (mostly younger in age); RE, Ross Embayment; RS, Ross Sea; WS, Weddell Sea; MBL, Marie Byrd Land; TI, Thurston Island; EWM, Ellsworth-Whitmore Mountains; and AP, Antarctic Peninsula.
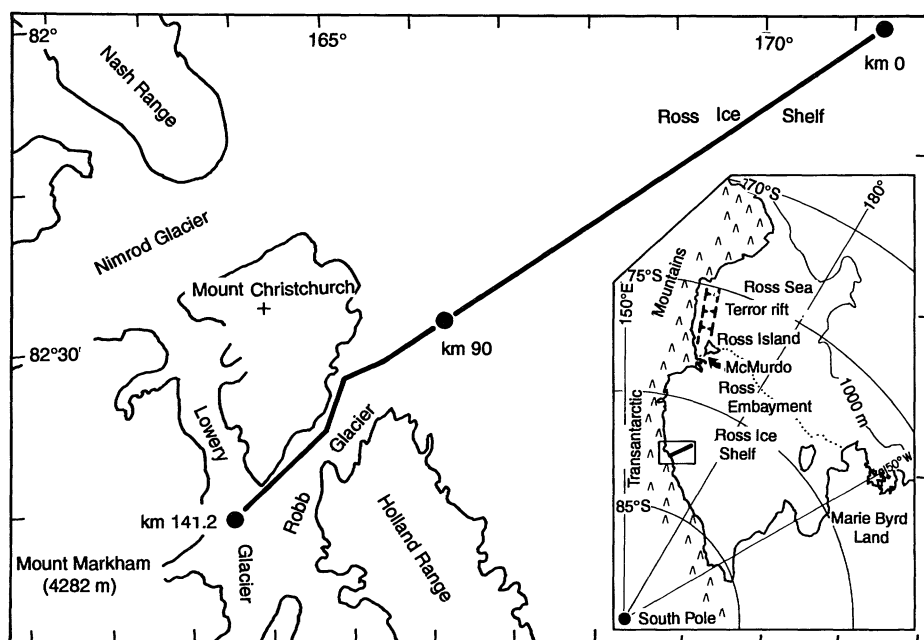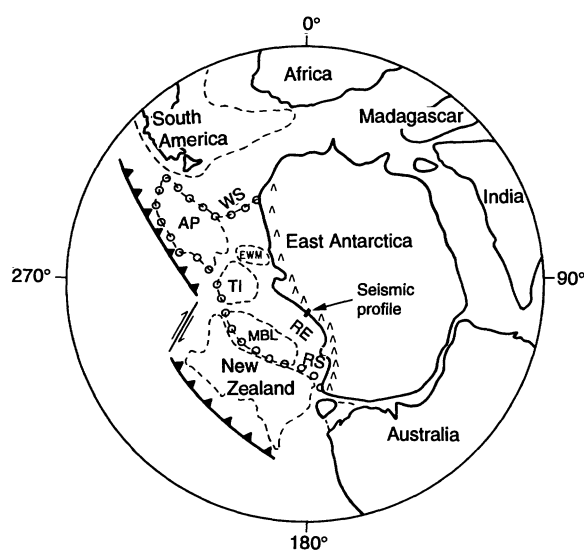

Fig. 2. Location map of the coincident seismic reflection and refraction and (inset) regional location map of the gravity profile across the boundary between the TAM and the Ross Embayment.
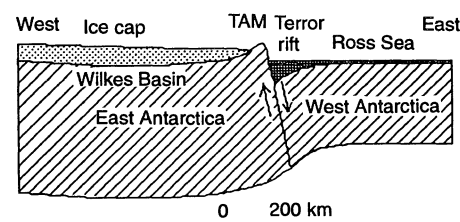
Fig. 3. Coupled uplift of TAM and subsidence of Terror rift along an inclined lithospheric boundary in a model where the East and West Antarctic lithospheres act as two elastic cantilevered beams (17).

Fig. 4. (Top) Seismic reflection profile and (bottom) interpretation (42). The sea floor is the uppermost reflection; BSR, bottom-simulating reflector marking the base of a gas-hydrate layer (43); A, B, and C are unconformities. Deeper primary arrivals could not be identified conclusively because of attenuation of seismic energy by the highly reflective ice-water and water-sediment interfaces.
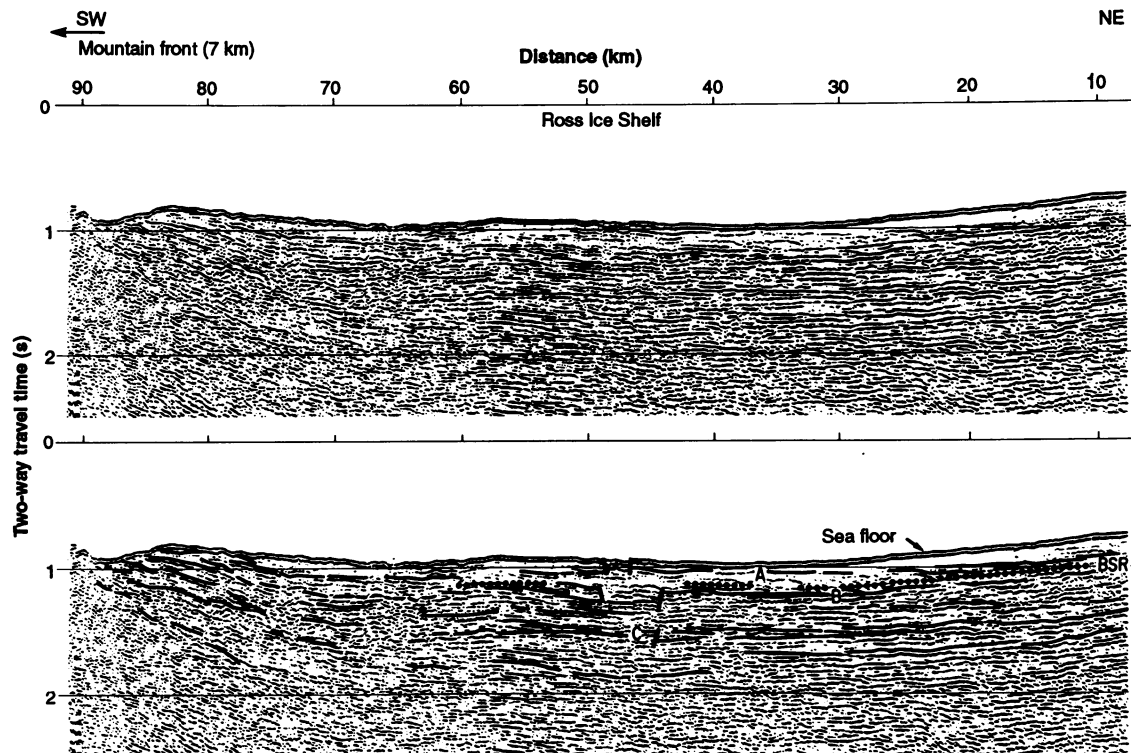
to its effective elastic thickness. There is a broad and shallow depression under the ice cover of East Antarctica, the Wilkes Basin, 500 km from the mountain front (1). The location of the Wilkes Basin suggests that the lithosphere has an effective elastic thickness of 110 ± 20 km (17). The large elastic thickness of the East Antarctic plate, one of the largest measured on Earth, is indicative of a thick lithosphere with a low geothermal gradient. In contrast, the Ross Embayment is characterized by a thinner lithosphere and a high geothermal gra-dient resulting from Mesozoic and Cenozoic stretching (12). Hence, large density and temperature contrasts probably occur across the boundary between the TAM and the Ross Embayment (14).

Data Acquisition and Interpretation

The only route across the boundary be-tween East and West Antarctica that ap-peared to be both crevasse-free and suitable for the scientific objectives was along the Robb Glacier, located about halfway be-tween the McMurdo station and the South Pole (Fig. 2). The 141-km-long traverse started on the glacier in the mountains and continued onto the ice shelf. We collected three types of data along the traverse: (i) multichannel seismic reflection data (18), which yield images of subsurface layers (Fig. 4); (ii) wide-angle seismic reflection and refraction data (19), which provide infor-mation on seismic velocities of the layers (Fig. 5) and can yield images of the deep crust (Fig. 6); and (iii) measurements of variations in the gravity field (20), which are indicative of variations in the densities of rocks in the subsurface (Fig. 7). The seismic velocities of layers are used to help determine the true depths of the reflection images and to infer the rock composition. Sound sources for both types of seismic data were dynamite charges placed at the bottom of 17-m-deep holes (21). Together, these data define the major sedimentary and crustal structures in the vicinity of the boundary between the rifted Ross Embay-ment and the TAM.

Sedimentary layers usually manifest themselves as continuous reflections. Tec-tonic activity of the crust can be traced by the progressive offset of these reflections and by differential thicknesses of sedimen-tary packages. The seismic reflection data from beneath the ice shelf (Fig. 4) show little evidence for tectonic activity and are interpreted to represent a glacial deposi-tional environment. The sediments show a complex internal stratigraphy, incoherent layering, and lenticular bodies similar to
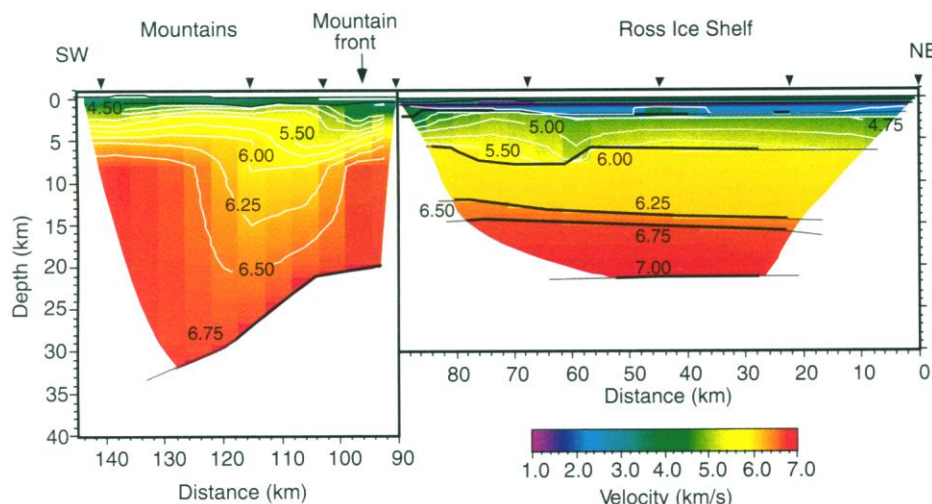
Fig. 5. Velocity-depth model of the sediments and crust along the SERIS profile from wide-angle reflection and refraction data (44). Triangles, shot points; heavy lines, boundaries generating reflections; colored area, the lateral extent of ray coverage; thin white lines, contours of P wave velocities at intervals of 0.25 km s^{-1}.

those of glacial deposits in the Ross Sea (22). Reflections close to the mouth of the Robb Glacier are truncated by the reflection of the sea floor, which suggests that the sea floor there is an erosional surface. Additionally, the high sediment velocity (2.1 to 2.5 km s^{-1}) immediately below the sea floor suggests that either there are no recently deposited sediments or that they were compacted by a grounded ice sheet. Three unconformities were observed in the sediments beneath the sea floor (Fig. 4). Similar unconformities in the Ross Sea are interpreted as the result of the waxing and waning of the ice sheet in the last 40 million years (12, 23).

The observed sedimentary reflections are subhorizontal except near the mouth of the

Robb Glacier, where they are slightly inclined (less than 3°) (Fig. 4). At kilometer 97, a subglacial escarpment ~500 m high with a ~45° slope marks the onset of the floating ice. This escarpment may mark a fault separating the TAM from the Ross Embayment. The mountains on both sides of the Robb Glacier also terminate against the ice shelf at about this location (Fig. 2). Thus, we define kilometer 97 as the subsurface expression of the mountain front. Beneath Robb Glacier, the ice-rock interface is rough on a scale of 1 km, and there is no evidence for the presence of sediments.

Because of logistical constraints, the wide-angle reflection and refraction profile, which provides a view of the deeper crustal structure, was split into a partially reversed

profile within the Ross Embayment (kilometers 0 to 90) and a fully reversed profile within the TAM (kilometers 90 to 141). The velocity-depth model (Fig. 5) derived from the seismic refraction data indicates that the sedimentary and crustal layers under the ice shelf (kilometers 0 to 90) are generally flat-lying. A thin (~1 km thick) layer of low-velocity sediments (<4 km s^{-1}) underlies the sea floor (24) and is probably of Tertiary age (25). The first refracted arrival under the ice shelf had a velocity of 4.5 to 5.5 km s^{-1} (associated with a density of 2550 kg m^{-3} in Fig. 7) and can be interpreted as either a high-velocity sedimentary rock layer or low-grade metasedimentary rock basement. A similar layer with a distinct refraction arrival was identified in the Ross Sea (25). The crystalline crust under the ice shelf is characterized by a strong midcrustal reflection at a depth of ~15 km. The depth to the seismically determined base of the crust (Moho) is 22 km, a depth similar to that found in the Ross Sea (25). The crustal structure under the mountains is different from that under the Ross Ice Shelf. There is no sedimentary layer below the grounded ice, and the upper crust has a high gradient in velocity. There is little evidence for a midcrustal reflection, despite the good quality of Moho arrivals (Fig. 6). Lower crustal velocities are typical of continental crust and are lower than those found under the Ross Ice Shelf. The crust gradually thickens from 22 km to between 30 and 35 km starting 0 to 10 km inland of the mountain front, as the base of the crust dips from 15° to 20° (Fig. 5). Unreversed seismic refraction data in the Ross Sea yielded a similar model in which the crust starts thickening offshore as its base dips at an angle of 10° (26).

The transition between the thin crust of the Ross Embayment and the thicker crust of East Antarctica is marked by a strong band of reflections that dip under the mountains (Fig. 6). The reflections, interpreted as the Moho, are remarkably continuous and unfaulted. In contrast, Moho reflections under the ice shelf are neither as strong nor as laminated. These differences may either be a result of a more severe attenuation of seismic energy or a crust-mantle boundary that is less prominent under the ice shelf than under the TAM. Laminated prominent Moho reflections beneath continental crust elsewhere have been interpreted as indicating cumulate layering (27), relatively undeformed metasedimentary rocks (27), the presence of pore fluids in rocks with a subhorizontal ductile fabric (28), layered intrusions (28), or increased scattering (29). Considering that the laminated reflections are tilted and similar reflections were not seen under the ice shelf, we interpret the reflections either

Fig. 6. Single-fold image of dipping Moho under the TAM front from wide-angle reflection data. Travel time was corrected with a hyperbolic moveout of 6 km s^{-1} (average crustal velocity) to approximate the geometry of the Moho. Abbreviations: I, direct wave within the ice layer; B, diving wave from the crystalline basement; and M, reflections from the crust-mantle interface (Moho). 1.
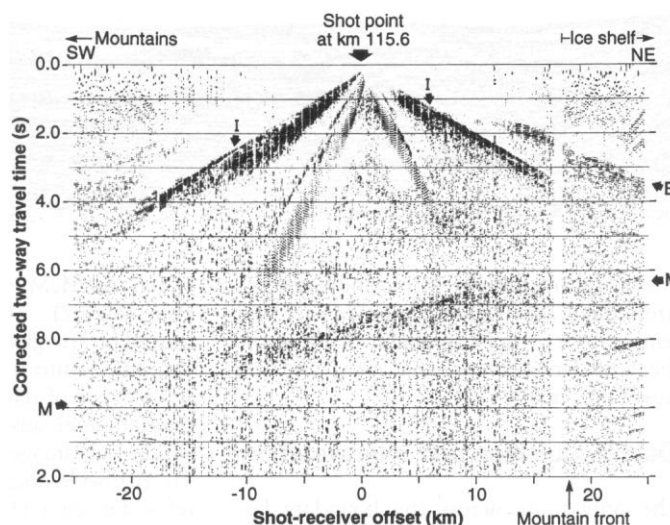
Fig. 7. (Top) Observed free-air gravity anomaly measured at 2-km intervals along the seismic line. (Bottom) Calculated gravity anomaly from a two-dimensional density-depth model; the model is based on the seismic results (Figs. 4 and 5).
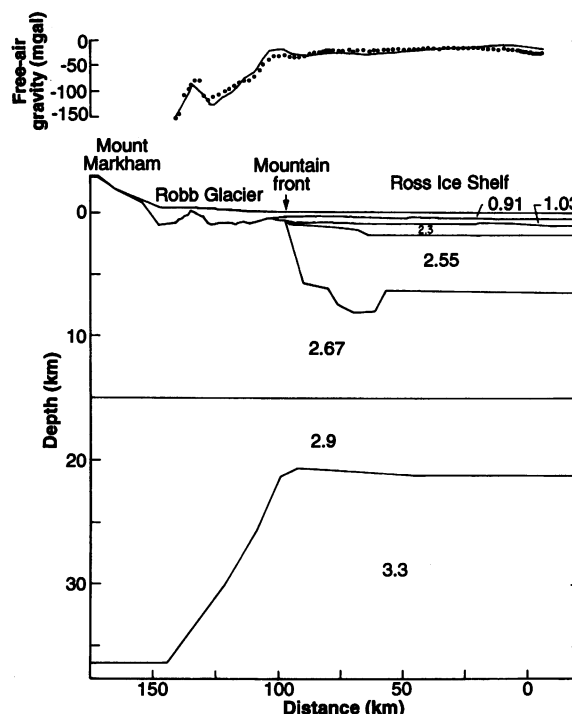
to represent a ductile fabric or to arise from increased scattering near the Moho.

The observed free-air gravity anomaly on the ice shelf (Fig. 7) varies by <10 mgal (1 mgal = 1 cm s^{-2}) (kilometers 0 to 86), as would be expected for a flat, undisturbed sedimentary and crustal structure. The anomaly decreases rapidly inland of the mountain front and has an average gradient of 2 to 3 mgal km^{-1}. The calculated gravity anomaly for a density model on the basis of the seismic reflection profile and the seismic refraction model (Fig. 7) agrees well with the observed gravity. Thus, the gravity data are consistent with the seismic interpretation.

The results of the SERIS experiment reveal that (i) there is no obvious sedimentary trough adjacent to the mountain front; (ii) the shallow sedimentary section shows little evidence of tectonic activity and is interpreted to have been glacially deposited; (iii) crustal thickness increases gradually from 20 to >30 km through a transition zone 40 km or more wide under the TAM; (iv) there is no indication of crustal underplating; and (v) crustal velocity structures under the ice shelf and under the mountains are different.

Tectonic Implications

These data provide a basis for understanding the transition between rifts and their margins in areas where rift-flank uplift develops. Isostatic and mechanical models of rift formation on both regional (30, 31) and local (32) scales postulate that uplift should be coupled to subsidence across normal faults and that the depth of the troughs should be at least equal to the height of the uplift. In this scenario, the late Cenozoic Terror rift and the bathymetric depression under the Ross Ice Shelf adjacent to the mountains (including the area under the SERIS line) (2) is the subsiding rift basin that is coupled to the uplift of the TAM (17, 33).

The results of the SERIS experiment show that these models are not tenable for the TAM and the Ross Ice Shelf. The bathymetric depression is not underlain by a significant graben, and the depression was most likely formed by glacial scouring. The sedimentary and crustal structures under the SERIS line in the Ross Embayment are flat for at least 100 km away from the mountain front, despite the proximity of the line to an area of the TAM that has undergone at least 5 km of uplift. The lateral extent of the flat crustal structure can be inferred from the Bouguer gravity field (2), which is uniform for 500 km along the mountain front between 81°S and 85°S. Farther to the north, the 300-km-long Terror rift (Fig. 2) terminates without a noticeable graben (25). Thus, not much of the

area adjacent to the 1500-km-long section of the TAM between 71°S and 85°S is underlain by a significant graben (Fig. 2). There is also no correlation along the Terror rift between the elevation of the TAM and the depth of the rift basin. Finally, the main phase of stretching of the Ross Embayment has preceded the uplift of the TAM by 20 million years or more.

The smooth dipping of the Moho from the Ross Embayment to the TAM (Fig. 6) indicates that the upper-mantle transition between the lithospheres of East and West Antarctica is gradual. In contrast, the transition within the crust, as deduced from the velocity structure, is abrupt. A strong crustal contrast is further supported by mineralogical and geochemical analyses of granulite xenoliths in the McMurdo area, which indicate that the composition of the lower crust under the TAM is significantly different from that under the Ross Embayment (34). Similarly, there appears to be a gradual transition in the upper mantle from the Basin and Range province to the Colorado Plateau in Arizona and an abrupt change in crustal structure (35). Thus, it appears that the stretched and hot upper mantle both at the Ross Embayment and at the Basin and Range extends somewhat into the surrounding regions, while the overlying crust is compositionally unaltered. In both areas, gradual transition in the upper mantle may reflect enhanced lateral thermal conduction or advection, compared to that in the crust or small-scale convection (36). As a result of enhanced heat flow toward the TAM, the buoyancy of the mantle lithosphere under the TAM is increased over its initial state and its thickness is decreased (14). The time delay between the stretching episode between West Antarctica and New Zealand and the uplift (as manifested in the fission track results) may reflect the gradual heating and alteration of the mantle lithosphere under the TAM. A related scenario for the uplift of the TAM is that the edge of East Antarctica drifted during the last 90 million years over the original position of the West Antarctic rift and was gradually heated (16).

The negligible evidence for either tectonic activity or mass wasting in the glacial sediments under the SERIS line is difficult to reconcile with the suggestion of a significant amount (2 to 3 km) of uplift of the TAM during the Pleistocene (13). Geological evidence also indicates insignificant amounts of recent uplift near McMurdo Sound (37, 38). We therefore suggest that the topography of the TAM was largely in place when Pleistocene glaciations took place. The enigma of the apparent aseismicity of Antarctica (39) and in particular along the TAM front may thus reflect the dearth of active uplift or subsidence. The

situation can be contrasted with that along the Wasatch front at the boundary of the Colorado Plateau and the Basin and Range province in Utah, where seismic activity accompanies the present uplift (40). The juvenile topography in parts of the TAM, therefore, probably resulted from low rates of erosion (41).

REFERENCES AND NOTES

1. D. J. Drewry, Glaciological and Geophysical Folio (Scott Polar Research Institute, Cambridge, United Kingdom, 1983).
2. L. L. Greischar, C. R. Bentley, L. R. Whiting, in Contributions to Antarctic Research, III, D. H. Elliot, Ed. (American Geophysical Union, Washington, DC, 1992), pp. 105–155.
3. D. D. Blankenship et al., Nature 361, 526 (1993).
4. Seismic surveys in Antarctica since the early reconnaissance traverses (1957 to 1967) include A. L. Kogan, in Antarctic Geology and Geophysics, R. J. Edie, Ed. (Universitetsforlaget, Oslo, 1972), pp. 485–489; A. Ikami, K. Ito, K. Shibuya, K. Kaminuma, in Antarctic Earth Sciences, R. L. Oliver, P. R. James, J. B. Jago, Eds. (Cambridge Univ. Press, Cambridge, 1983), pp. 509–513; D. D. Blankenship, C. R. Bentley, S. T. Rooney, R. B. Alley, Nature 322, 54 (1986); A. Hungeling and F. Thyssen, in Geological Evolution of Antarctica, M. R. A. Thomson, J. A. Crane, J. W. Thomson, Eds. (Cambridge Univ. Press, Cambridge), pp. 73–76; E. C. King and E. P. Jarvis, First Break 9, 281 (1991); B. C. Beaudoin, U. S. ten Brink, T. A. Stern, Geophysics 57, 1359 (1992); and C. G. Munson and C. R. Bentley, in Recent Progress in Antarctic Earth Sciences, Y. Yoshida, K. Kaminuma, K. Shiraishi, Eds. (TERRAPUB, Tokyo, in press). None of the previous surveys matched the scale or used the modern techniques that were used in this experiment.
5. L. A. Lawver, J.-Y. Royer, D. T. Sandwell, C. R. Scotese, in Geological Evolution of Antarctica, M. R. A. Thomson, J. A. Crane, J. W. Thomson, Eds. (Cambridge Univ. Press, Cambridge, 1991), pp. 533–539.
6. A. M. Grunow et al., J. Geophys. Res. 96, 17935 (1991).
7. D. L. Schmidt and P. D. Rowley, Tectonics 5, 279 (1986).
8. J. Stock and P. Molnar, Nature 325, 495 (1987).
9. J. D. Bradshaw, Tectonics 8, 803 (1989).
10. R. M. Carter, N. Z. J. Geol. Geophys. 31, 405 (1988).
11. Both are submerged under several hundred meters of water and are unusually thin for a continental crust [20 to 25 km (12); R. G. Allis, Tectonics 5, 15 (1986); M. Reiner, personal communication].
12. A. K. Cooper, F. J. Davey, K. Hinz, in Geological Evolution of Antarctica, M. R. A. Thomson, J. A. Crane, J. W. Thomson, Eds. (Cambridge Univ. Press, Cambridge, 1991), pp. 285–291.
13. J. C. Behrendt and A. Cooper, Geology 19, 315 (1991).
14. U. S. ten Brink and T. A. Stern, J. Geophys. Res. 97, 569 (1992).
15. E. Stump and P. G. Fitzgerald, Geology 20, 161 (1992).
16. A. G. Smith and D. J. Drewry, Nature 309, 536 (1984).
17. T. A. Stern and U. S. ten Brink, J. Geophys. Res. 94, 10315 (1989).
18. These data were recorded with a 1.5-km-long snow streamer (borrowed from Norsk-Hydro, Bergen, Norway). The snow streamer is a towed seismic cable to which 60 groups of gimballed geophones are connected at 25-m intervals [O. Eiken, M. Degutsch, P. Riste, K. Rod, First Break 7, 374 (1989)]. Use of the snow streamer resulted in a substantial increase in the acquisition rate compared to that from conventional seismic work on land, without compromising the data quality.
19. Wide-angle seismic data are recorded many kilometers away from the shot, here up to 90 km.

These data were digitally recorded by stand-alone units [borrowed from Incorporated Research Institutions for Seismology (IRIS), Washington, DC] arranged in arrays 25 km long with receiver intervals of 100 to 300 m.
20. Gravity was measured by a Worden (Texas Instruments, Houston, TX) gravimeter and tied to the McMurdo gravity base station. The observed gravity anomaly was found to be within 0.5 mgal of that from a previous regional survey (2). Relative elevations along the profile were measured by pairs of barometers.
21. Holes were drilled by melting of the ice with hot water pumped under pressure. For the multichannel reflection work, 7.5-kg charges were spaced every 200 m along the profile. Two charges 1.6 km apart were detonated for each streamer location. This pattern resulted in an effective 120-channel receiving array 3 km long. The sources for the wide-angle reflection and refraction data were several explosions of 100 to 400 kg.
22. L. R. Bartek, P. R. Vail, J. B. Anderson, P. A. Emmet, S. Wu, J. Geophys. Res. 96, 6753 (1991).
23. K. Hinz and M. Block, in Proceedings of the 11th World Petroleum Congress (Wiley, New York, 1984), pp. 279–291.
24. Velocities directly beneath the sea floor were less than that of solid ice (3.8 km s⁻¹) and therefore produced no refracted arrivals. For this portion of the refraction model (beneath the sea floor under the ice shelf), velocities were obtained from the stacking velocities of the reflection data.
25. A. K. Cooper and F. J. Davey, The Antarctic Continental Margin: Geology and Geophysics of the Western Ross Sea [Circum-Pacific Council for Energy and Mineral Resources (CPCEMR), Houston, 1987].
26. D. R. H. O'Connell and T. M. Stepp, in Geol. Jahrb., in press.
27. L. D. Hale and G. A. Thompson, J. Geophys. Res. 87, 4625 (1982).
28. R. Meissner and N. J. Kusznir, Ann. Geophys. Ser. B 5, 365 (1987).
29. B. S. Gibson and A. R. Levander, Geophys. Res. Lett. 15, 617 (1988).
30. W. A. Heiskanen and F. A. Vening Meinesz, The Earth and its Gravity Field (McGraw-Hill, New York, 1958).
31. J. Braun and C. Beaumont, Geology 17, 760 (1989).
32. R. S. Stein, G. C. P. King, J. B. Rundle, J. Geophys. Res. 93, 13319 (1988).
33. M. H. P. Bott and T. A. Stern, Tectonophysics 201, 341 (1992).
34. R. I. Kalamarides, J. H. Berg, R. A. Hank, Science 237, 1192 (1987).
35. E. B. Goodwin and J. McCarthy, J. Geophys. Res. 95, 20097 (1990).
36. W. R. Buck, Earth Planet. Sci. Lett. 77, 362 (1986).
37. P. J. Barrett, M. J. Hambrey, D. M. Harwood, A. R. Pyne, P.-N. Webb, DSIR Bull. 245, 241 (1989).
38. C. M. Clapperton and D. E. Sugden, Quat. Sci. Rev. 9, 253 (1990).
39. A. C. Johnston, Nature 330, 467 (1987).
40. G. Zandt and G. Owens, Bull. Seismol. Soc. Am. 70, 1501 (1980).
41. P. Wellman and R. J. Tingey, Nature 291, 142 (1981).
42. The stacked profile was enhanced by the combination of four adjacent traces and the application of a two-dimensional median filter and was not migrated.
43. The BSR here shares similar characteristics with BSRs identified and drilled in low-latitude margins: It simulates the sea floor, cuts across stratigraphic units, exhibits a polarity reversal of the wavelet compared to the sea floor, and is overlain by an acoustically opaque layer. Bottom-simulating reflectors are caused by a thin layer of free gas at the base of a gas hydrate–cemented layer. Methane gas has been encountered in drill holes and cores around Antarctica, but despite the anomalously large depth of the Antarctic shelves, BSRs have rarely been documented [K. A. Kvenvolden, M. Golan-Bac, J. B. Rapp, in The Antarctic Continental Margin: Geology and Geophysics of Offshore Wilkes Land, S. L. Eittreim and M. A. Hampton, Eds. (CPCEMR, Houston, 1987), pp. 205–213].
44. We modeled the refraction data using both forward- and inverse-ray tracing programs [J. H. Luetgert, U.S. Geol. Surv. Open-File Rep. 88-238 (1988), p. 52; W. J. Lutter, R. L. Nowack, L. W. Braile, J. Geophys. Res. 95, 4621 (1990)]. Values for ice thickness and absolute elevation from previous regional surveys of the Ross Ice Shelf [D. G. Albert and C. R. Bentley, in The Ross Ice Shelf: Glaciology and Geophysics, C. R. Bentley and D. E. Hayes, Eds. (American Geophysical Union, Washington, DC, 1990), pp. 87–108] were used for modeling of the refraction and gravity data.
45. We thank R. Busby, B. Harris, S. Heaphy, T. Hefford, C. Hobbs, N. Lord, D. Lousley, and B. Straite for their invaluable help in the field; Polar Ice Coring Office, (University of Alaska, Fairbanks) for drilling the shot holes; A. Melhuish, M. Lee, W. Agena, W. Poag, W. Dillon, and J. Zwinakis for helping with processing, interpretation, and drafting; P. Barrett, C. Bentley, F. Davey, D. Hutchinson, K. Klitgord, G. Thompson, and one anonymous individual for helpful reviews; Norsk-Hydro, Y. Kristoffersen, and E. Rygg for lending the snow streamer; Grant-Norpac (Houston, TX) for lending computer boards; and IRIS for sending a technician and lending stand-alone recording units and peripherals. Funded by National Science Foundation grant DPP89-17634 and the New Zealand Science Foundation.

RESEARCH ARTICLES

Three-Dimensional Structure of Myosin Subfragment-1: A Molecular Motor

Ivan Rayment,* Wojciech R. Rypniewski,† Karen Schmidt-Bäse,‡ Robert Smith, Diana R. Tomchick,§ Matthew M. Benning, Donald A. Winkelmann, Gary Wesenberg, Hazel M. Holden

Directed movement is a characteristic of many living organisms and occurs as a result of the transformation of chemical energy into mechanical energy. Myosin is one of three families of molecular motors that are responsible for cellular motility. The three-dimensional structure of the head portion of myosin, or subfragment-1, which contains both the actin and nucleotide binding sites, is described. This structure of a molecular motor was determined by single crystal x-ray diffraction. The data provide a structural framework for understanding the molecular basis of motility.

Motility is one of the characteristic features of many living organisms and involves the transduction of chemical into mechanical energy. Only a limited number of strategies have evolved to accomplish this task. At present, three major classes of molecular motors have been identified, myosin, dynein, and kinesin, and all are important in cellular movement (1). Of these three proteins, the most abundant is myosin, which plays both a structural and an enzymatic role in both muscle contraction and intracellular motility.

I. Rayment, W. R. Rypniewski, K. Schmidt-Bäse, R. Smith, D. R. Tomchick, M. M. Benning, G. Wesenberg, and H. M. Holden are in the Department of Biochemistry and Institute for Enzyme Research, University of Wisconsin, 1710 University Avenue, Madison, WI 53705. D. A. Winkelmann is in the Department of Pathology, Robert Wood Johnson Medical School, Piscataway, NJ 08854.

*To whom all correspondence should be addressed.
†Present address: European Molecular Biology Laboratory, Notkestrasse 85, 2000 Hamburg 52, Germany.
‡Present address: Max Planck Institute for Biochemistry, 8033 Martinsried, Germany.
§Present address: Department of Biological Sciences, Purdue University, West Lafayette, IN 47907.

The role of myosin in movement has been most clearly defined from the study of cross-striated skeletal muscle, which shows a high degree of structural organization. In striated muscle the basic contractile unit is the sarcomere, which consists of overlapping arrays of thick and thin filaments. During contraction, these filaments, which are composed primarily of myosin and actin, respectively, slide past one another, thereby shortening the length of the sarcomere (2). Electron micrographs of muscle in rigor have revealed connections between the filaments in the overlap region, the so-called crossbridges. These crossbridges are formed by the globular regions of the myosin molecule and are responsible for force generation in the contractile process through the hydrolysis of adenosine triphosphate (ATP).

Myosin, which has a molecular size of about 520 kilodaltons, consists of two 220-kD heavy chains and two pairs of light chains that vary in molecular size depending on the source but are usually between 15 and 22 kD (3, 4). The molecule is highly